International Journal of Engineering, Mathematical and Physical Sciences
ISSN: 2517-9934
Vol:5, No:12, 2011

Autonomous Control of a Mobile Manipulator

Shonal Singh, Bibhya Sharma and Jito Vanualailai

***Abstract*—**This paper considers the design of a motion planner that will simultaneously accomplish control and motion planning of a *n*-link nonholonomic mobile manipulator, wherein, a *n*-link holonomic manipulator is coupled with a nonholonomic mobile platform, within an obstacle-ridden environment. This planner, derived from the Lyapunov-based control scheme, generates collision-free trajectories from an initial configuration to a final configuration in a constrained environment cluttered with stationary solid objects of different shapes and sizes. We demonstrate the efficiency of the control scheme and the resulting acceleration controllers of the mobile manipulator with results through computer simulations of an interesting scenario.

***Keywords*—**Artificial potential fields, Lyapunov-based control scheme, Lyapunov stability, nonholonomic manipulator, minimum distance technique, kinodynamic constraints.

I. Introduction

THE autonomous navigation of mechanical systems in obstacle-ridden, or real-world, environments has been an active research domain for at least three decades now. A plethora of control architectures appear in literature for generating control laws governing the motion of various different robotic systems in constrained environments. Of the many mechanical systems appearing in literature, a classical example is the mobile manipulator, where the manipulator is mounted on a wheeled platform. Such a combined system, which incorporates the functions of a conventional robotic manipulator and a mobile robotic base, inherits the dexterity of the manipulator and the increased workspace of the mobile base, and can cover a wide spectrum of engineering applications including explorations, surveillance, mining and construction [1]. Also, these articulated robots are capable of performing wide-ranging tasks in various different environments, which may be hazardous or even inaccessible to humans [2].

The pioneer work of Seraji in the 1990s [3] is now considered as a landmark result in the literature of motion planning and control of mobile manipulators. Seraji's milestone result was based on the meticulous development of a set of differential kinematic equations governing the motion of a mobile manipulator by efficaciously combining the nonholonomic base constraints, the desired end-effector motion, and the redundancy resolution goals. Since its inception in the 1990s, the repository of research aimed at mobile manipulators has grown enormously and continues to do so, and has expanded to include applications that require the development of efficient motion planners for a wide range of mobile manipulators operating in obstacle-ridden environments. The reader is referred to [2] and the references therein for a detailed account of noteworthy contributions in this field in the last two decades.

In this paper, we extend the results of [2] to a *n*-link nonholonomic mobile manipulator and endeavor in designing acceleration controls of the robotic system within the framework of the control scheme adopted from [2]. The control scheme, classified as a Lyapunov-based control scheme, is an algorithmic amalgamation of the principles of the Direct Method of Lyapunov and artificial potential fields. The pivotal idea behind this control scheme is to design an appropriate Lyapunov function which acts as an artificial potential field function or *total potentials*. Accordingly, the scheme warrants the attachment of an attractive (or positive) field to the target and a repulsive (or negative) field to each obstacle, with the direction of motion facilitated via notion of steepest descent [2]. In parallel, the scheme also addresses stability issues of the system via the integrated Lyapunov Method.

The rest of the paper is organized as follows: in Section II, the kinodynamic model of the *n*-link nonholonomic mobile manipulator is derived using Cartesian coordinates; in Section III, we deploy the Lyapunov-based control scheme by designing attractive and repulsive potential field functions; in Section IV, the acceleration controllers are designed and stability analysis of the mobile manipulator system carried out; in Section V, computer simulation of an interesting scenario is presented; and Section VI concludes the paper and outlines future work in the area.

II. System Modelling

The *n*-link nonholonomic mobile manipulator, which we shall hereafter denote as *n*MM, $n \in \mathbb{N}$, consists of a nonholonomic rear wheel car-like mobile platform with a *n*-link planar arm mounted on the mid-front axle of the platform. As an illustration, we have provided the schematics of a 4-link mobile manipulator, or 4MM, see Fig. 1.

With reference to Fig. 1, at time $t \geq 0$, $\left(x(t), y(t)\right)$ denotes the position of the end-effector, $\phi(t)$ corresponds to the platform's steering angle with respect to its longitudinal axis, while ℓ_0 and b_0 are, respectively, the length and the width of the platform. Furthermore, ℓ_k is the length of link k, $k \in \{1, 2, \ldots, n\}$. The reader is referred to Table I for a

S. Singh is with the School of Computing, Information and Mathematical Sciences, Faculty of Science, Technology and Environment, The University of the South Pacific, Suva, Fiji Islands, and e-mail: (see singh_sb@usp.ac.fj).
S. Singh, B. Sharma and J. Vanualailai are with The University of the South Pacific.

description of the variables that will be used to depict the kinodynamic model of the manipulator system with respect to the Cartesian position of the end-effector in the z_1z_2 plane.

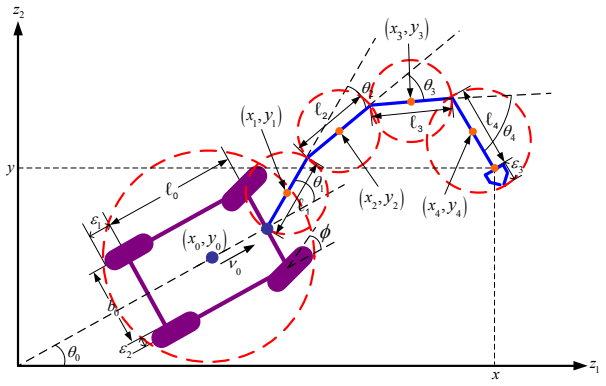

Fig. 1 Schematics of a 4MM

TABLE I
NOMENCLATURE OF THE MOBILE MANIPULATOR SYSTEM

Variable	Description
$x_0(t)$	z_1 component of the position of the center of the platform
$y_0(t)$	z_2 component of the position of the center of the platform
$x_k(t)$	z_1 component of the position of the center of link k
$y_k(t)$	z_2 component of the position of the center of link k
$\theta_0(t)$	angular position of platform with respect to the z_1 axis
$\theta_1(t)$	angular position of link 1 with respect to the platform
$\theta_k(t)$	angular position of link k with respect to link $k-1$, $k=2,3,\ldots,n$
$v_0(t)$	linear velocity of the wheels of the platform
$\omega_0(t)$	angular velocity of the platform
$\omega_k(t)$	angular velocity of link k
$u_1(t)$	linear acceleration of the wheels of the platform
$u_2(t)$	angular acceleration of the platform
$u_{k+2}(t)$	angular acceleration of link k

For clarity, we will now consider the governing equations of the nonholonomic mobile platform and the n-link planar arm separately and then combine them effectively to obtain the governing ODEs of the complete nMM.

A. Nonholonomic Wheeled Platform

We consider a rear-wheel driven car-like robot model as the wheeled platform, whereby engine power is applied to the rear wheels. The wheeled platform resides in a disk of radius r_0 and is positioned at center (x_0,y_0), and is described by the set $A=\{(z_1,z_2)\in\mathbb{R}^2:(z_1-x_0)^2+(z_2-y_0)^2\le r_0^2\}$.

Adopting the nomenclature of [4], if we let M be the mass of A, F the force along the axis of A, Γ the torque about a vertical axis at (x_0,y_0) and I the moment of inertia of A, then the kinodynamic model of the wheeled platform with respect to its center $(x_0,y_0)\in\mathbb{R}^2$ is (on suppressing t)

$$\begin{aligned}\dot{x}_0&=v_0\cos\theta_0-\tfrac{1}{2}\ell_0\omega_0\sin\theta_0,\\ \dot{y}_0&=v_0\sin\theta_0+\tfrac{1}{2}\ell_0\omega_0\cos\theta_0,\\ \dot{\theta}_0&=\omega_0,\\ \dot{v}_0&=u_1:=F/M,\\ \dot{\omega}_0&=u_2:=\Gamma/I,\end{aligned}\qquad(1)$$

where u_1 and u_2 are, respectively, the instantaneous translational and rotational accelerations of the platform.

Additionally, as per the nomenclature of [2], [4], we assume no slippage, that is,

$$\dot{x}_r\sin\theta_0-\dot{y}_r\cos\theta_0=0,$$

and

$$\dot{x}_f\sin(\theta_0+\phi)-\dot{y}_f\cos(\theta_0+\phi)=0,$$

and pure rolling, that is,

$$\dot{x}_0\cos\theta_0+\dot{y}_0\sin\theta_0=v_0,$$

where (x_r,y_r) and (x_f,y_f) are the Cartesian coordinates of the rear and front wheels of A, respectively. These generate non-integrable constraints of the wheeled platform, constraints that are denoted as the *nonholonomic constraints* of system (1).

B. n-Link Manipulator

We now consider an-link fully actuated arm. Suppose that link 1 is anchored at $(0,0)$, the origin of the z_1z_2 plane, then the position (x,y) of the end-effector is given by the following equations:

$$x=\sum_{k=1}^{n}\ell_k\cos\left(\sum_{p=1}^{k}\theta_p\right),$$
$$y=\sum_{k=1}^{n}\ell_k\sin\left(\sum_{p=1}^{k}\theta_p\right).$$

Thus, we derive the kinodynamic model of the n-link arm with respect to the position of the end-effector $(x,y)\in\mathbb{R}^2$ as (on suppressing t)

$$\dot{x} = -\sum_{k=1}^{n}\sum_{i=1}^{k}\left[\ell_k \sin\left(\sum_{p=1}^{k}\theta_p\right)\right]\omega_i,$$
$$\dot{y} = \sum_{k=1}^{n}\sum_{i=1}^{k}\left[\ell_k \cos\left(\sum_{p=1}^{k}\theta_p\right)\right]\omega_i,$$
$$\dot{\theta}_k = \omega_k,$$
$$\dot{\omega}_k = u_{k+2},$$

where ω_k and u_{k+2} are the instantaneous angular velocities and accelerations, respectively, of the various bodies of the manipulator, for $k \in \{1,2,\ldots,n\}$.

C. n-Link Mobile Manipulator

Now we consider the nonholonomic mobile platform and the *n*-link manipulator as one complete robotic unit. The position of the end-effector, denoted as $(x,y) \in \mathbb{R}^2$, with respect to the platform center $(x_0,y_0) \in \mathbb{R}^2$ is

$$x = x_0 + \tfrac{\ell_0}{2}\cos\theta_0 + \sum_{k=1}^{n}\ell_k \cos\left(\sum_{p=0}^{k}\theta_p\right),$$
$$y = y_0 + \tfrac{\ell_0}{2}\sin\theta_0 + \sum_{k=1}^{n}\ell_k \sin\left(\sum_{p=0}^{k}\theta_p\right).$$

Differentiating x and y implicitly with respect to time $t \geq 0$ (on suppressing t) yields the instantaneous velocity components $(\dot{x},\dot{y})$, and as such, the kinodynamic model of the *n*MM with respect to the position of the end-effector $(x,y) \in \mathbb{R}^2$ is then derived as

$$\begin{aligned}\dot{x} &= v_0\cos\theta_0 - \sum_{m=0}^{n}\left[\ell_m \sin\left(\sum_{p=0}^{m}\theta_p\right)\right]\omega_0 \\ &\quad - \sum_{m=1}^{n}\left[\sum_{k=m}^{n}\ell_k \sin\left(\sum_{p=0}^{k}\theta_p\right)\right]\omega_m, \\ \dot{y} &= v_0\sin\theta_0 + \sum_{m=0}^{n}\left[\ell_m \cos\left(\sum_{p=0}^{m}\theta_p\right)\right]\omega_0 \\ &\quad + \sum_{m=1}^{n}\left[\sum_{k=m}^{n}\ell_k \cos\left(\sum_{p=0}^{k}\theta_p\right)\right]\omega_m, \\ \dot{\theta}_m &= \omega_m, \\ \dot{v}_0 &= u_1, \\ \dot{\omega}_m &= u_{m+2},\end{aligned} \tag{2}$$

where $m \in \{0,1,2,\ldots,n\}$. System (2) is a description of the instantaneous velocities and accelerations of the *n*MM. We shall use the vector notation $\mathbf{x} = (x,y,\theta_0,\theta_1,\theta_2,\ldots,\theta_n,v_0,\omega_0,\omega_1,\omega_2,\ldots,\omega_n) \in \mathbb{R}^{2n+5}$ to refer to the position and velocity components of the *n*MM in the z_1z_2 plane.

It can be observed that we can express the positions of the mobile platform and link k, where $k \in \{1,2,\ldots,n\}$, of the *n*MM completely in terms of the state variables; hence for the wheeled platform, we have

$$\left.\begin{aligned} x_0 &= x - \tfrac{\ell_0}{2}\cos\theta_0 - \sum_{k=1}^{n}\tfrac{\ell_k}{2^{\frac{1}{|k+1|}}}\cos\left(\sum_{p=0}^{k}\theta_p\right), \\ y_0 &= y - \tfrac{\ell_0}{2}\sin\theta_0 - \sum_{k=1}^{n}\tfrac{\ell_k}{2^{\frac{1}{|k+1|}}}\sin\left(\sum_{p=0}^{k}\theta_p\right),\end{aligned}\right\} \tag{3}$$

and for the n links, we have

$$\left.\begin{aligned} x_m &= x - \sum_{k=m}^{n}\tfrac{\ell_k}{2^{\frac{|m+1|}{|k+1|}}}\cos\left(\sum_{p=0}^{k}\theta_p\right), \\ y_m &= y - \sum_{k=m}^{n}\tfrac{\ell_k}{2^{\frac{|m+1|}{|k+1|}}}\sin\left(\sum_{p=0}^{k}\theta_p\right),\end{aligned}\right\} \tag{4}$$

where $m = 1,2,\ldots,n$. These position constraints are known as the *holonomic constraints* of the mobile manipulator system.

III. Deployment of the Control Scheme

Our primary objective is to derive artificial potential field functions (APFs), and accordingly, design the translational and rotational accelerations, u_1 and u_{m+2}, for $m \in \{0,1,2,\ldots,n\}$, respectively, within the framework of the Lyapunov-based control scheme, such that the *n*MM will be able to carry out a number of subtasks before reaching its destination. The subtasks include: navigating in the static but obstacle-ridden environment; respecting the kinematic and dynamic constraints, and reaching the target position safely. The proposed APFs are distance functions formed in Euclidian space and the control scheme combines these APFs to form a Lyapunov function candidate – a platform to design the nonlinear controllers for the *n*MM. This Lyapunov function candidate will also be utilized in a later section to prove stability of the kinodynamic system.

The APFs will be designed in the following subsections; the attractive APFs for convergence and target attraction, and the repulsive APFs that repel the robot from specified obstacles.

A. Target Attraction

We affix a target for the robot to reach after some time $t > 0$. For the end-effector of the *n*MM, we have a designated target with center (p_1,p_2) and radius rt, and we define this target as $T = \left\{(z_1,z_2) \in \mathbb{R}^2 : (z_1-p_1)^2 + (z_2-p_2)^2 \leq rt^2\right\}$.

For attraction to this target, we utilize the target attractive function

$$V(\mathbf{x}) = \frac{1}{2}\left[(x-p_1)^2 + (y-p_2)^2 + v_0^2 + \sum_{j=0}^{n}\omega_j^2\right],$$

which is not only a measure of the Euclidian distance between the end-effector of the mobile manipulator but is also a measure of its convergence to the target [2].

B. Kinematic Constraints

The kinematic constraints are the nonholonomy of the *n*MM and fixed or moving obstacles in the workspace. While the various nonholonomic constraints of the robotic system are reflected in the dynamic model governed by system (2), the fixed obstacles are the four boundaries of the rectangular workspace, and the solid obstacles fixed within the workspace.

To ensure that the entire body of the *n*MM safely steers past an obstacle, we enclose each articulated body of the robot by the smallest circle possible. Once more, as an illustration, we have provided the procedural schematics of the protective regions for a 4MM, see Fig. 1. Given the *clearance parameters* ε_1 and ε_2, we can enclose the platform by a circular protective region centered at (x_0, y_0) with radius $r_0 = \frac{1}{2}\sqrt{(\ell_0 + 2\varepsilon_1)^2 + (b_0 + 2\varepsilon_2)^2}$. For link k, we use a circular protective region centered at (x_k, y_k) with radius $r_k = \frac{\ell_k}{2}$, where $k = 1,2,\ldots,n-1$. Moreover, for link n, we use a circular protective region centered at (x_n, y_n) with radius $r_n = \frac{\ell_n}{2} + \varepsilon_3$ (where ε_3 is the *safety parameter* needed to protect the gripper). This methodology essentially emulates a well-known technique in mobile robot path-planning schemes, wherein the robot is portrayed as a simpler fixed-shaped object [5].

1) Workspace: Boundary Limitations

We adopt a planar workspace, which is a fixed, closed, and bounded rectangular region defined for $\eta_1, \eta_2 > 2\sum_{m=0}^{n} r_m$, as $WS = \{(z_1, z_2) \in \mathbb{R}^2 : 0 \le z_1 \le \eta_1,\ 0 \le z_2 \le \eta_2\}$. The region's boundaries are defined as follows:

Left Boundary: $B_1 = \{(z_1, z_2) \in \mathbb{R}^2 : z_1 = 0\}$;

Lower Boundary: $B_2 = \{(z_1, z_2) \in \mathbb{R}^2 : z_2 = 0\}$;

Right Boundary: $B_3 = \{(z_1, z_2) \in \mathbb{R}^2 : z_1 = \eta_1\}$;

Upper Boundary: $B_4 = \{(z_1, z_2) \in \mathbb{R}^2 : z_2 = \eta_2\}$.

Each of these boundary lines will be considered as fixed obstacles, which have to be avoided by each articulated body of the robot at all time $t \ge 0$, so that the mobile manipulator is confined within the four boundaries of the workspace. Hence, for the avoidance by the wheeled platform and the n links, we shall adopt the following obstacle avoidance functions for the avoidance of the left, lower, right and upper boundaries, respectively:

$$W_{4m+1}(\mathbf{x}) = x_m - r_m,$$
$$W_{4m+2}(\mathbf{x}) = y_m - r_m,$$
$$W_{4m+3}(\mathbf{x}) = \eta_1 - (r_m + x_m),$$
$$W_{4m+4}(\mathbf{x}) = \eta_2 - (r_m + y_m),$$

for $m = 0,1,2,\ldots,n$. Since $\eta_1, \eta_2 > 2\sum_{m=0}^{n} r_m$, each of the aforementioned functions is positive in WS. That is, $W_{4m+1}(\mathbf{x}), W_{4m+3}(\mathbf{x}) > 0$ for all $x_m \in (r_m, \eta_1 - r_m)$ and $W_{4m+2}(\mathbf{x}), W_{4m+4}(\mathbf{x}) > 0$ for all $y_m \in (r_m, \eta_2 - r_m)$, recalling that the components of (x_m, y_m) are given in equations (3) and (4).

To generate repulsive effects from the function W_s, $s = 1,2,\ldots,4n+4$, we design a repulsive potential field function which is an inverse function that encodes the avoidance function to the denominator and a *tuning parameter* $\alpha_s > 0$ in the numerator. This ratio acts to restrict the articulated robot to operate within its rectangular workspace.

Henceforth, all the obstacle avoidance functions will be appropriately coupled with tuning parameters, in accordance with the Lyapunov-based control scheme, to design the repulsive potential field functions to generate the obstacle avoidance maneuvers of the *n*MM. The reader is referred to [2] for a detailed anecdote of the effects of the obstacle avoidance functions and the resulting repulsive potential field functions.

2) Stationary Solid Objects

Category 1: Elliptical Obstacles

Let us fix $q \in \mathbb{N}$ stationary objects, or obstacles, within the boundaries of WS. We assume that the l th obstacle is an ellipse in *nonstandard position* with center (o_{l1}', o_{l2}'). Precisely, the l th elliptical obstacle is *the nonstandard set* $E_l' = \left\{(z_1', z_2') \in \mathbb{R}^2 : \frac{(z_1' - o_{l1}')^2}{A_l^2} + \frac{(z_2' - o_{l2}')^2}{B_l^2} \le 1\right\}$, where the $z_1'z_2'$ plane is measured with respect to the z_1z_2 plane. In essence, the $z_1'z_2'$ plane is obtained by rotating the z_1z_2 plane counterclockwise through the angle ψ_l. Also, the center (o_{l1}', o_{l2}') is with respect to the $z_1'z_2'$ plane.

The relationships (called *rotation equations*) between the two planes can be given by $z_1' = z_1 \cos\psi_l + z_2 \sin\psi_l$ and $z_2' = -z_1 \sin\psi_l + z_2 \cos\psi_l$. Also, $o_{l1}' = o_{l1}\cos\psi_l + o_{l2}\sin\psi_l$ and $o_{l2}' = -o_{l1}\sin\psi_l + o_{l2}\cos\psi_l$, where (o_{l1}, o_{l2}) is the center of the l th elliptical obstacle with respect to the z_1z_2 plane. Now,

$$z_1' - o_{l1}' = (z_1 - o_{l1})\cos\psi_l + (z_2 - o_{l2})\sin\psi_l,$$

and

$$z_2' - o_{l2}' = -(z_1 - o_{l1})\sin\psi_l + (z_2 - o_{l2})\cos\psi_l.$$

Therefore, the set E_l' can be rewritten with respect to the z_1z_2 plane as

$$E_l = \{(z_1, z_2) \in \mathbb{R}^2 : A_l' + B_l' \le 1\},$$

where

$$A_l^{'} = \frac{\left[(z_1 - o_{l1})\cos\psi_l + (z_2 - o_{l2})\sin\psi_l\right]^2}{A_l^2},$$

$$B_l^{'} = \frac{\left[-(z_1 - o_{l1})\sin\psi_l + (z_2 - o_{l2})\cos\psi_l\right]^2}{B_l^2}.$$

We note that when $\psi_l = 0$, the l th elliptical obstacle is in *standard position* such that a *horizontal ellipse* is when $A_l > B_l$ and a *vertical ellipse* is when $A_l < B_l$. Moreover, if $A_l = B_l$ (for all values of ψ_l), the ellipse collapses into a circle with radius $A_l = B_l$.

For the avoidance of the l th obstacle, we will need to have separate avoidance functions for all m bodies of the nMM. Thus, we consider the obstacle avoidance function

$$EO_{ml}(\mathbf{x}) = \frac{1}{2}\left[\hat{A}_{ml} + \hat{B}_{ml} - 1\right],$$

where

$$\hat{A}_{ml} = \frac{\left[(x_m - o_{l1})\cos\psi_l + (y_m - o_{l2})\sin\psi_l\right]^2}{(A_l + r_m)^2},$$

$$\hat{B}_{ml} = \frac{\left[-(x_m - o_{l1})\sin\psi_l + (y_m - o_{l2})\cos\psi_l\right]^2}{(B_l + r_m)^2},$$

for $m = 0,1,2,\ldots,n$ and $l = 1,2,\ldots,q$. The function $EO_{ml}(\mathbf{x})$ is the measure of the Euclidian distance between the center of the l th obstacle and the m th articulated body of the nMM and has the same effect as the aforementioned repulsive functions.

Category 2: Rod-shaped Obstacles

Let us fix $z \in \mathbb{N}$ rod-shaped obstacles within WS. Adopting the methodology of [2], we assume that the $\tilde{k}$ th rod-shaped obstacle can be collapsed into a straight line segment with initial coordinates $(a_{\tilde{k}1}, b_{\tilde{k}1})$ and final coordinates $(a_{\tilde{k}2}, b_{\tilde{k}2})$. Precisely, the $\tilde{k}$ th rod-shaped obstacle is the set $S_{\tilde{k}} = \left\{(z_1, z_2) \in \mathbb{R}^2 : (z_1 - c_{m\tilde{k}}) + (z_2 - d_{m\tilde{k}})\right\}$, where $c_{m\tilde{k}} = a_{\tilde{k}1} + \lambda_{m\tilde{k}}(a_{\tilde{k}2} - a_{\tilde{k}1})$ and $d_{m\tilde{k}} = b_{\tilde{k}1} + \lambda_{m\tilde{k}}(b_{\tilde{k}2} - b_{\tilde{k}1})$ is its parametric representation, for $0 \le \lambda_{m\tilde{k}} \le 1$ and $m = 0,1,2,\ldots,n$.

Utilizing the minimum distance technique of [2] we identify the closest point of each $\tilde{k}$ th line segment measured from the reference point of the m th body of the nMM. The avoidance of the closest point at any time $t \ge 0$ essentially results in the avoidance of the entire line segment by the complete nMM. Minimizing the Euclidian distance between the point (x_m, y_m) and the $\tilde{k}$ th line segment $(c_{m\tilde{k}}, d_{m\tilde{k}})$ yields

$$\lambda_{m\tilde{k}} = (x_m - a_{\tilde{k}1})q_{\tilde{k}1} + (y_m - b_{\tilde{k}1})q_{\tilde{k}2},$$

with

$$q_{\tilde{k}1} = \frac{a_{\tilde{k}2} - a_{\tilde{k}1}}{(a_{\tilde{k}2} - a_{\tilde{k}1})^2 + (b_{\tilde{k}2} - b_{\tilde{k}1})^2},$$

$$q_{\tilde{k}2} = \frac{b_{\tilde{k}2} - b_{\tilde{k}1}}{(a_{\tilde{k}2} - a_{\tilde{k}1})^2 + (b_{\tilde{k}2} - b_{\tilde{k}1})^2}.$$

In this research, we utilize a *saturation function* $\lambda_{m\tilde{k}} : \mathbb{R}^2 \to [0,1] \subset \mathbb{R}$ given as

$$\lambda_{m\tilde{k}}(c_{m\tilde{k}}, d_{m\tilde{k}}) = \begin{cases} 0 & , \text{ if } \lambda_{m\tilde{k}} < 0, \\ \lambda_{m\tilde{k}} & , \text{ if } 0 \le \lambda_{m\tilde{k}} \le 1, \\ 1 & , \text{ if } \lambda_{m\tilde{k}} > 1. \end{cases}$$

We note that $\lambda_{m\tilde{k}}(c_{m\tilde{k}}, d_{m\tilde{k}})$ is a nonnegative scalar such that it is restricted to the interval $[0,1]$, implying that there is always an avoidance of the $\tilde{k}$ th rod-shaped obstacle at every iteration $t \ge 0$.

For the avoidance of these category of obstacles fixed in the workspace, we will need to again have separate avoidance functions for the platform and the n links. Thus, we design

$$RO_{m\tilde{k}}(\mathbf{x}) = \frac{1}{2}\left[(x_m - c_{m\tilde{k}})^2 + (y_m - d_{m\tilde{k}})^2 - r_m^2\right],$$

for $m = 0,1,2,\ldots,n$ and $\tilde{k} = 1,2,\ldots,z$. The function $RO_{m\tilde{k}}(\mathbf{x})$ is the measure of the distance between the closest point of the $\tilde{k}$ th rod-shaped obstacle and the center of the m th articulated body of the nMM.

C. Artificial Obstacles from Dynamic Constraints

The instantaneous velocities of the mobile platform and the n links are restricted due to safety considerations, and the rotation angles of link k, for $k = 1,2,\ldots,n$, are restricted due to mechanical singularities. The only way these dynamic constraints can be treated within the Lyapunov-based control scheme is to construct *artificial obstacles* associated to each constraint and then avoid them to yield the desired effect.

1) Modulus Bound on Velocities

From a practical viewpoint, the translational and rotational velocities of the manipulator system are limited, so we include additional constraints:

(i) $|v_0| < v_{\max}$, where $v_{\max}$ is the *maximal achievable speed*;

(ii) $|\omega_0| < \frac{v_{\max}}{|\rho_{\min}|}$, where $\rho_{\min} = \frac{\ell_0}{\tan(\phi_{\max})}$. This condition arises due to the boundness of the steering angle ϕ. That is, $|\phi| \le \phi_{\max}$, where $\phi_{\max}$ is the *maximal steering angle*;

(iii) $|\omega_m| < \omega_{m\max}$, for $m = 1,2,\ldots,n$, where $\omega_{m\max}$ is the *maximal rotational velocity* of link m of the n-link arm.

Based on these constraints, we design an artificial obstacle tagged to each constraint. For example, we construct the artificial obstacle $AO_1 = \left\{v_0 \in \mathbb{R} : v_0 \le -v_{\max} \text{ or } v_0 \ge v_{\max}\right\}$, to cater for the maximal achievable speed.

For the avoidance of these artificial obstacles, we design the following obstacle avoidance functions, respectively:

$$U_1(\mathbf{x}) = \frac{1}{2}(v_{\max} - v_0)(v_{\max} + v_0),$$
$$U_2(\mathbf{x}) = \frac{1}{2}\left(\frac{v_{\max}}{|\rho_{\min}|} - \omega_0\right)\left(\frac{v_{\max}}{|\rho_{\min}|} + \omega_0\right),$$
$$U_{m+2}(\mathbf{x}) = \frac{1}{2}\left(\omega_{m\max} - \omega_m\right)\left(\omega_{m\max} + \omega_m\right).$$

These positive functions would guarantee the adherence to the limitations placed upon the steering angle and the velocities when encoded appropriately into the tentative Lyapunov function.

2) Mechanical Singularities

A singular configuration arises when $\theta_m = 0$, $\theta_m = \pi$ or $\theta_m = -\pi$, for $m = 2,3,\ldots,n$. Consequently, the condition placed on θ_m is $0 < |\theta_m| < \pi$, which means that the links can neither be fully stretched nor folded onto each other. Based on the aforementioned singular configurations, we construct the following functions:

$$S_{2m-3}(\mathbf{x}) = |\theta_m|, \quad S_{2m-2}(\mathbf{x}) = \pi - |\theta_m|,$$

for $\theta_m \in (-\pi, 0) \cup (0, \pi)$ and $m = 2,3,\ldots,n$. Each function will be used to avoid the artificial obstacle defined as $AO_{m+(n+1)} = \{\theta_m \in \mathbb{R} : \theta_m = 0,\ \theta_m = \pi \text{ or } \theta_m = -\pi\}$.

We also note that the angle between link 1 and the mobile platform is bounded, that is, $-\pi/2 < \theta_1 < \pi/2$. In other words, link 1 can freely rotate within $(-\pi/2, \pi/2)$. To ensure that link 1 stays within this interval, we will use

$$S_{2n-1}(\mathbf{x}) = \frac{1}{2}\left(\frac{\pi}{2} - \theta_1\right)\left(\frac{\pi}{2} + \theta_1\right),$$

for the avoidance of the artificial obstacle defined as $AO_{2n+2} = \{\theta_1 \in \mathbb{R} : \theta_1 \le -\pi/2 \text{ or } \theta_1 \ge \pi/2\}$.

D. Auxiliary Function

To guarantee the convergence of the *n*MM to its prescribed target and to ensure that the nonlinear controllers vanish at this target configuration, an attractive function whose role is purely mathematical, and hence auxiliary, is designed. This function will be multiplied to each of the aforementioned obstacle avoidance functions. Thus, it suffices to consider

$$F(\mathbf{x}) = \frac{1}{2}\left[(x - p_1)^2 + (y - p_2)^2\right],$$

as an appropriate auxiliary function.

IV. Lyapunov-Based Control Scheme

This section essays the extraction of the nonlinear control laws of system (2) via the Lyapunov-based control scheme. In parallel, the control scheme will in turn utilize Lyapunov's Direct Method to provide mathematical proof of stability of system (2).

We begin with the following theorem:

Theorem 1: Consider the *n*-link mobile manipulator whose motion is governed by ODEs described in system (2). The objective is to, amongst other integrated subtasks, control the motion of the robot within an obstacle-ridden environment. The subtasks include: restrictions placed on the workspace, convergence to a predefined target, and consideration of kinodynamic constraints. Utilizing the aforementioned potential field functions the following continuous acceleration controllers can be generated for the *n*MM that per se guarantees stability, in the sense of Lyapunov, of system (2) as well:

$$\left.\begin{aligned} u_1 &= -(\delta_1 v_0 + G_1)/\, g_{n+1}, \\ u_{m+2} &= -(\delta_{m+2}\omega_m + G_{m+2})/\, g_{n+(m+2)}, \end{aligned}\right\}$$

where $m \in \{0,1,2,\ldots,n\}$ and $\delta_i > 0$, for $i = 1,2,\ldots,n+2$, are constants commonly known as *convergence parameters*.

Proof of Stability: Combining all the attractive and repulsive potential functions and introducing *tuning parameters* (or *control parameters*), $\alpha_s > 0$, $\gamma_{ml} > 0$, $\sigma_{m\tilde{k}} > 0$, $\xi_p > 0$, and $\beta_r > 0$, where $s,l,\tilde{k},p,r \in \mathbb{N}$ and $m = 0,1,2,\ldots,n$, we define a Lyapunov function candidate for system (2) as

$$L(\mathbf{x}) = V(\mathbf{x}) + F(\mathbf{x})\sum_{s=1}^{4n+4}\frac{\alpha_s}{W_s(\mathbf{x})} + F(\mathbf{x})\sum_{m=0}^{n}\sum_{l=1}^{q}\frac{\gamma_{ml}}{EO_{ml}(\mathbf{x})} + F(\mathbf{x})\sum_{m=0}^{n}\sum_{\tilde{k}=1}^{z}\frac{\sigma_{m\tilde{k}}}{RO_{m\tilde{k}}(\mathbf{x})} + F(\mathbf{x})\left(\sum_{p=1}^{2n-1}\frac{\xi_p}{S_p(\mathbf{x})} + \sum_{r=1}^{n+2}\frac{\beta_r}{U_r(\mathbf{x})}\right).$$

Then the following assumption is made:

Assumption 1: If a fixed point $\mathbf{x}^* = (p_1, p_2, \theta_0, \theta_1, \theta_2, \ldots, \theta_n, 0,0,0,0,\ldots,0) \in \mathbb{R}^{2n+5}$, then $\mathbf{x}^* \in D(L(\mathbf{x}))$ is, at least, an equilibrium state for the kinodynamic system (2).

Remark 1: If $\dot{L}(\mathbf{x}) = f(\mathbf{x})$, then $f(\mathbf{x}^*) = 0$ making $\mathbf{x}^*$ a feasible equilibrium point, at least, in a small neighborhood of the target configuration.

Then one can easily verify the following:

1) $L(\mathbf{x})$ is defined, continuous and positive over the domain $D(L(\mathbf{x})) = \{W_s(\mathbf{x}) > 0; EO_{ml}(\mathbf{x}) > 0; RO_{m\tilde{k}}(\mathbf{x}) > 0; S_p(\mathbf{x}) > 0; U_r(\mathbf{x}) > 0\}$;
2) $L(\mathbf{x}^*) = 0$;
3) $L(\mathbf{x}) > 0\ \forall \mathbf{x} \in D(L(\mathbf{x}))/\mathbf{x}^*$.

Now consider the time derivative of the Lyapunov function candidate along a particular trajectory of system (2):

$$\dot{L}(\mathbf{x}) = f_1\dot{x}_1 + f_2\dot{y}_2 + \sum_{m=1}^{n} g_m\dot{\theta}_m + \sum_{m=0}^{n}\left(f_{2m+3}\dot{x}_m + f_{2m+4}\dot{y}_m\right) + g_{n+1}v_0\dot{v}_0 + \sum_{m=0}^{n} g_{n+(m+2)}\omega_m\dot{\omega}_m,$$

where, for $m = 0,1,2,\ldots,n$ (on suppressing $\mathbf{x}$)

$$f_1 = \left[1 + \sum_{s=1}^{4n+4}\frac{\alpha_s}{W_s} + \sum_{m=0}^{n}\left(\sum_{l=1}^{q}\frac{\gamma_{ml}}{EO_{ml}} + \sum_{\tilde{k}=1}^{z}\frac{\sigma_{m\tilde{k}}}{RO_{m\tilde{k}}}\right) + \sum_{p=1}^{2n-1}\frac{\xi_p}{S_p} + \sum_{r=1}^{n+2}\frac{\beta_r}{U_s}\right](x - p_1),$$

$$f_2 = \left[1 + \sum_{s=1}^{4n+4}\frac{\alpha_s}{W_s} + \sum_{m=0}^{n}\left(\sum_{l=1}^{q}\frac{\gamma_{ml}}{EO_{ml}} + \sum_{\tilde{k}=1}^{z}\frac{\sigma_{m\tilde{k}}}{RO_{m\tilde{k}}}\right) + \sum_{p=1}^{2n-1}\frac{\xi_p}{S_p} + \sum_{r=1}^{n+2}\frac{\beta_r}{U_s}\right](y - p_2),$$

$$f_{2m+3} = -F\left\{\frac{\alpha_{4m+1}}{W_{4m+1}^2} - \frac{\alpha_{4m+3}}{W_{4m+3}^2} + \sum_{l=1}^{q}\frac{\gamma_{ml}}{EO_{ml}^2}\left[\frac{(x_m - o_{l1})\cos\psi_l + (y_m - o_{l2})\sin\psi_l}{(A_l + r_m)^2}\right]\cos\psi_l - \sum_{l=1}^{q}\frac{\gamma_{ml}}{EO_{ml}^2}\left[\frac{(y_m - o_{l2})\cos\psi_l - (x_m - o_{l1})\sin\psi_l}{(B_l + r_m)^2}\right]\sin\psi_l\right\} - F\sum_{\tilde{k}=1}^{z}\frac{\sigma_{m\tilde{k}}}{RO_{m\tilde{k}}^2}\left\{(x_m - c_{m\tilde{k}})\left[1 - (a_{\tilde{k}2} - a_{\tilde{k}1})q_{\tilde{k}1}\right]\right\} + F\sum_{\tilde{k}=1}^{z}\frac{\sigma_{m\tilde{k}}}{RO_{m\tilde{k}}^2}\left\{(y_m - d_{m\tilde{k}})\left[1 - (b_{\tilde{k}2} - b_{\tilde{k}1})q_{\tilde{k}1}\right]\right\},$$

$$f_{2m+4} = -F\left\{\frac{\alpha_{4m+2}}{W_{4m+2}^2} - \frac{\alpha_{4m+4}}{W_{4m+4}^2} + \sum_{l=1}^{q}\frac{\gamma_{ml}}{EO_{ml}^2}\left[\frac{(x_m - o_{l1})\cos\psi_l + (y_m - o_{l2})\sin\psi_l}{(A_l + r_m)^2}\right]\sin\psi_l + \sum_{l=1}^{q}\frac{\gamma_{ml}}{EO_{ml}^2}\left[\frac{(y_m - o_{l2})\cos\psi_l - (x_m - o_{l1})\sin\psi_l}{(B_l + r_m)^2}\right]\cos\psi_l\right\} - F\sum_{\tilde{k}=1}^{z}\frac{\sigma_{m\tilde{k}}}{RO_{m\tilde{k}}^2}\left\{(y_m - d_{m\tilde{k}})\left[1 - (b_{\tilde{k}2} - b_{\tilde{k}1})q_{\tilde{k}2}\right]\right\} + F\sum_{\tilde{k}=1}^{z}\frac{\sigma_{m\tilde{k}}}{RO_{m\tilde{k}}^2}\left\{(x_m - c_{m\tilde{k}})\left[1 - (a_{\tilde{k}2} - a_{\tilde{k}1})q_{\tilde{k}2}\right]\right\},$$

$$g_1 = \frac{\xi_{2n-1}F}{S_{2n-1}^2}\theta_1,$$

$$g_{n+1} = 1 + \frac{\beta_1 F}{U_1^2}, \quad g_{n+(m+2)} = 1 + \frac{\beta_{m+2}F}{U_{m+2}^2}.$$

Furthermore, for $m = 2,3,\ldots,n$

$$g_m = -F\left(\frac{\xi_{2m-3}}{S_{2m-3}^2} - \frac{\xi_{2m-2}}{S_{2m-2}^2}\right)\frac{|\theta_m|}{\theta_m}.$$

Defining $g_0 = 0$ and letting

$$G_1 = \left(f_1 + \sum_{m=0}^{n} f_{2m+3}\right)\cos\theta_0 + \left(f_2 + \sum_{m=0}^{n} f_{2m+4}\right)\sin\theta_0,$$

$$G_{m+2} = -\ell_m\left(f_1 + \frac{1}{2}f_{2m+3}\right)\sin\left(\sum_{p=0}^{m}\theta_p\right) + \ell_m\left(f_2 + \frac{1}{2}f_{2m+4}\right)\cos\left(\sum_{p=0}^{m}\theta_p\right) - \ell_m\sum_{k=m+1}^{n} f_{2k+3}\sin\left(\sum_{p=0}^{m}\theta_p\right) + \ell_m\sum_{k=m+1}^{n} f_{2k+4}\cos\left(\sum_{p=0}^{m}\theta_p\right) + g_m,$$

for $m = 0,1,2,\ldots,n$ and substituting the controllers given in Theorem 1 and the governing ODEs for system (2) one secures a semi-negative definite function

$$\dot{L}(\mathbf{x}) = -\left(\delta_1 v_0^2 + \sum_{m=0}^{n}\delta_{m+1}\omega_m^2\right) \le 0.$$

Thus, $\dot{L}(x) \le 0 \ \forall x \in D(L(\mathbf{x}))$ and $\dot{L}(\mathbf{x}^*) = 0$. Finally, it can be easily verified that the first partials of $L(\mathbf{x})$ is C^1, which makes up the fifth and final prerequisite of a Lyapunov function, and consequently, $\mathbf{x}^*$ is, at least, a stable equilibrium point in the sense of Lyapunov.

In the current work, this practical limitation is well within the Lyapunov framework and there is no contradiction with Brockett's Theorem [6] because only stability has been proven and not asymptotic stability.

V. Simulation Results

In this section, we demonstrate simulation results for a 3-link mobile manipulator (that is, $n = 3$) navigating in a constrained workspace cluttered with fixed obstacles. We verify numerically the stability results obtained from the Lyapunov function.

We have fabricated a traffic situation wherein the 3MM has to maneuver from an initial state to a final state, whilst avoiding multiple elliptical and rod-shaped obstacles. The workspace contains $q = 20$ elliptical obstacles, each with random positions and sizes. The parameter γ_{ml} has been randomized between 1 and 5, where $m = 0,1,2,3$ and $l = 1,2,\ldots,20$. Additionally, the workspace is cluttered with $z = 20$ rod-shaped obstacles, each with random initial and final coordinates. The associated parameter $\sigma_{m\tilde{k}}$ has been

randomized between 0 and 1, where $m = 0,1,2,3$ and $\tilde{k} = 1,2,\ldots,20$. Note that the corresponding initial and final states, workspace restrictions, numerical values of the different parameters and other essentials required to simulate the scenario are listed in Table II.

TABLE II
NUMERICAL VALUES OF INITIAL STATES, CONSTRAINTS AND PARAMETERS

Initial Configuration	
Rectangular position	$(x, y) = (5,5)$
Angular positions	$\theta_0 = 0$, $\theta_1 = \pi/3$, $\theta_2 = -\pi/4$, $\theta_3 = -\pi/4$
Translational velocity	$v_0 = 1$
Rotational velocities	$\omega_0 = \omega_1 = \omega_2 = \omega_3 = 0.05$
Constraints	
Dimension of robot	$\ell_0 = 1.8$, $b_0 = 0.8$, and $\ell_1 = \ell_2 = \ell_3 = 0.8$
Target	center $(p_1, p_2) = (49,45)$, and radius $rt = 0.5$
Max. velocities	$v_{\max} = 5$, $\omega_{1\max} = 1$, $\omega_{2\max} = 1$, $\omega_{3\max} = 1$
Max. steering angle	$\phi_{\max} = 7\pi/18$
Clearance parameters	$\varepsilon_1 = \varepsilon_2 = 0.1$, $\varepsilon_3 = 0.2$
WS boundaries	$\eta_1 = 50$, $\eta_2 = 50$
Elliptical obstacles	$(o_{l1}, o_{l2}) \in \{[3,\eta_1 - 3],[3,\eta_2 - 3]\}$, $(A_l, B_l) \in \{[0,3],[0,3]\}$, $\psi_l \in [-\pi,\pi]$, for $l = 1,\ldots,20$
Rod obstacles	$a_{\tilde{k}1} \in [4,\eta_1 - 4]$, $b_{\tilde{k}1} \in [4,\eta_2 - 4]$, $a_{\tilde{k}2} \in [a_{\tilde{k}1} + 4, a_{\tilde{k}1} - 4]$, $b_{\tilde{k}2} \in [b_{\tilde{k}1} + 4, b_{\tilde{k}1} - 4]$, for $\tilde{k} = 1,\ldots,20$
Parameters	
Boundary limitations	$\alpha_s = 1$, for $s = 1,\ldots,16$
Obstacle avoidance	$\gamma_{ml} \in [1,5]$, for $l = 1,\ldots,20$ and $\sigma_{m\tilde{k}} \in [0,1]$, for $\tilde{k} = 1,\ldots,20$, where $m = 0,\ldots,3$
Dynamic constraints	$\xi_p = 0.5$, $\beta_r = 2.5$, for $p = 1,\ldots,5$ and $r = 1,\ldots,5$
Convergence	$\delta_i = 500$, for $i = 1,\ldots,5$

The nonlinear controllers u_i, for $i = 1,2\ldots,5$, weresimulated to generate a feasible robot trajectory, as seen in Fig. 2. With the initial conditions described in Table II, the control laws ensured a nice convergence of the system state tothe equilibrium state, whilst satisfying all underlying constraints.

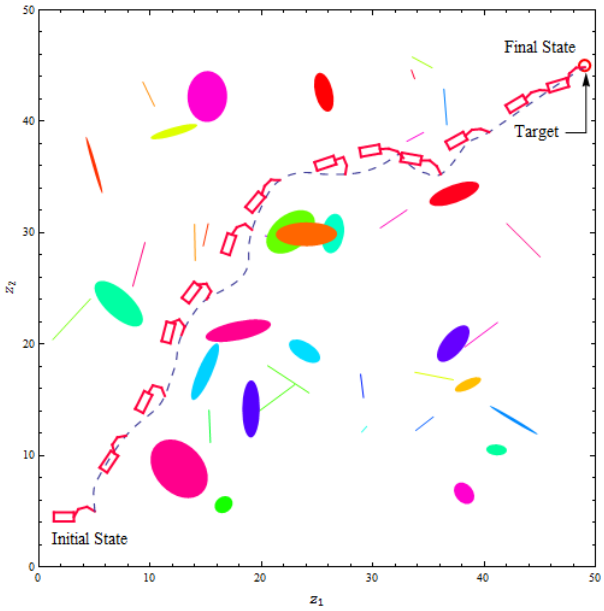

Fig. 2 Trajectory of the 3MM within a constrained environment

Fig. 3 shows the evolution of the Lyapunov function and its time derivative along the system trajectory. Not only does the figure show that the conditions of Theorem 1 have been satisfied but it also gives us information on where the 3MM accelerated or decelerated. As shown in the figure, an increase in $\dot{L}(\mathbf{x})$ indicates that the 3MM is decelerating, where as a decrease in $\dot{L}(\mathbf{x})$ indicates that the 3MM is accelerating.

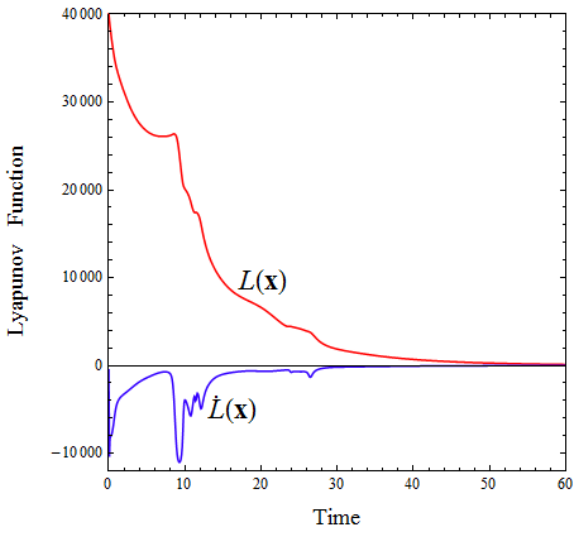

Fig. 3 Lyapunov function $L(\mathbf{x})$ and its time derivative $\dot{L}(\mathbf{x})$

Fig. 4 shows the behavior of the linear and angular velocities of the platform. Clearly, the translational velocity of the platform decreases as it approaches a fixed obstacle and gains speed rapidly once it avoids collision with a fixed obstacle. Finally, the 3MM slows down on approach to the target and eventually, at the center of the target the linear and angular velocities vanish. The behavior of the rotational velocities of the 3 links of the manipulator is shown in Fig. 5, which also tend to zero as the robot approaches the target. We have also provided the orientations of the various bodies of the 3MM as it traverses towards its final state, see Fig. 6.

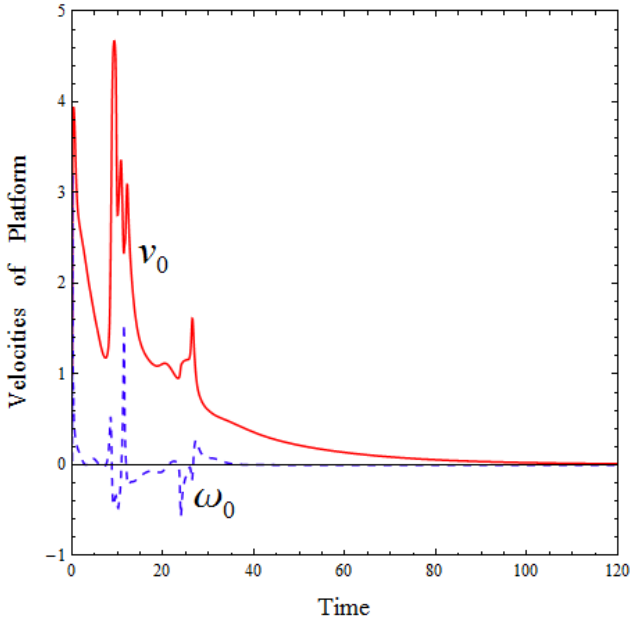

Fig. 4 Velocities of the wheeled platform

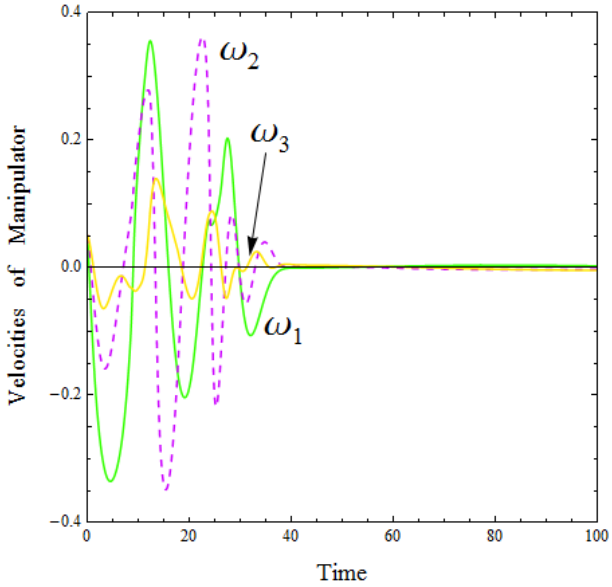

Fig. 5 Rotational velocities of the three links

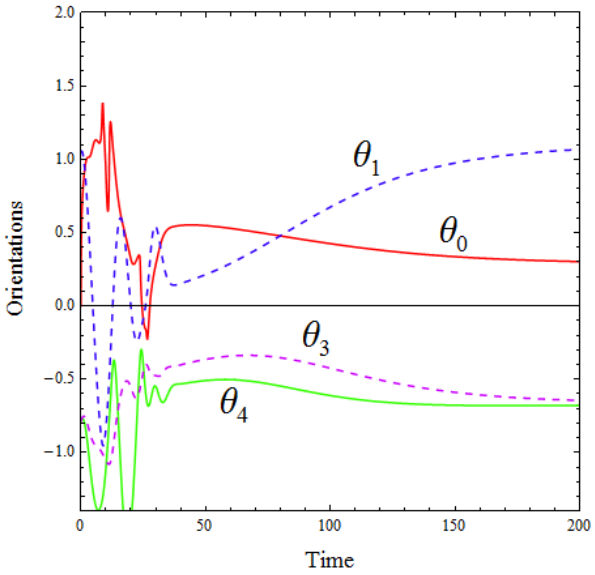

Fig. 6 Orientations of the various articulated bodies of the 3MM

Fig. 7 and Fig. 8 show explicitly the time evolution of the relevant nonlinear controllers along the trajectory of the 3MM. One can clearly notice the convergence of these controllers at the final configuration implying the effectiveness of the acceleration controllers.

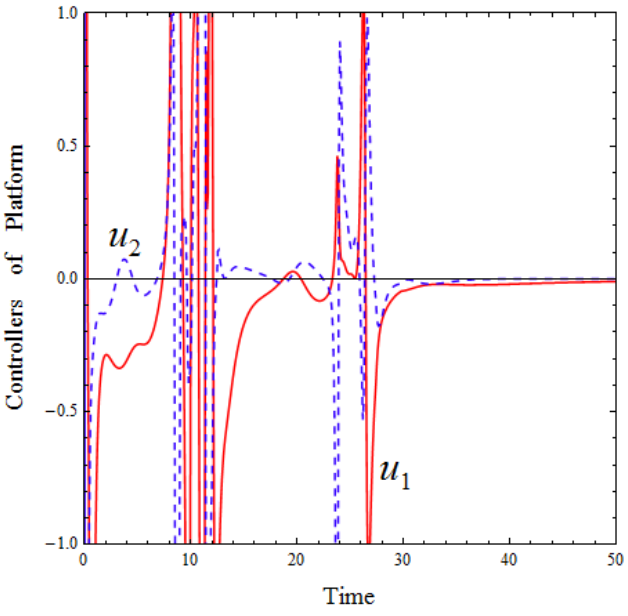

Fig. 7 Controllers of the wheeled platform

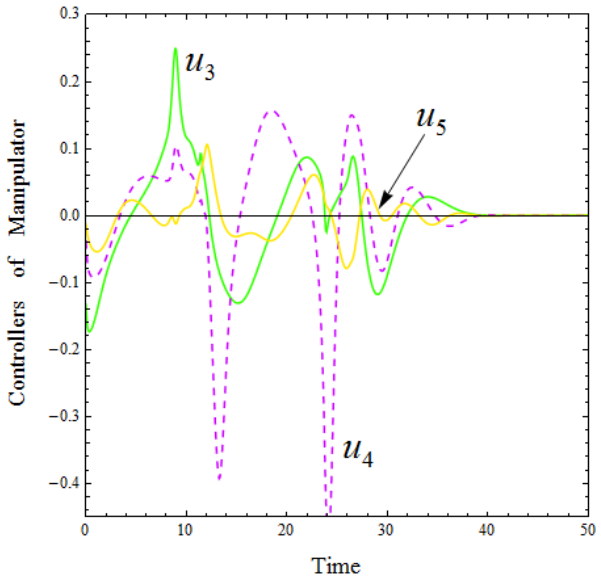

Fig. 8 Controllers of the three links

VI. Conclusion

This paper presents a set of continuous, time-invariant acceleration control laws, derived from the Lyapunov-based control scheme, to tackle the problem of autonomous navigation of a *n*-link nonholonomic mobile manipulator in a workspace cluttered with elliptical and rod-shaped obstacles of different sizes and orientations. In addition, this approach guaranteed the stability of the system in the sense of Lyapunov. The efficiency of the control laws has been verified through computer simulations of a 3MM operating within a virtual environment.

Future work includes fine tuning the trajectories by parameter optimization, extending the proposed technique to doubly nonholonomic mobile manipulators and modifying the proposed control algorithm for motion planning in dynamic environments, which include moving obstacles other than mobile robots.

References

[1] J. J. Craig, "Introduction to Robotics: Mechanics and Control," in *The Mechanics and Control of Mechanical Manipulators*, 2nd ed., Wesley Publishing Company, Inc., 1989, pp. 111–114.

[2] B. Sharma, "New Directions in the Applications of the Lyapunov-based Control Scheme to the Findpath Problem," PhD dissertation, The University of the South Pacific, 2008.

[3] H. Seraji, "A Unified Approach to Motion Control of Mobile Manipulators,"*International Journal of Robotics Research*, vol. 2, pp. 107–118, 1998.

[4] B. Sharma, J. Vanualailai and U. Chand, "Flocking of Multi-agents in Constrained Environments," *European Journal of Pure and Applied Mathematics*, vol. 3, pp. 401–425, 2009.

[5] P. C-Y and Q. Xue, "Intelligent Robotic Planning Systems," *World Scientific*, Singapore, 1993.

[6] R. W. Brockett,*Differential Geometry Control Theory*. New York: Springer-Verlag, 2003, ch. Asymptotic Stability and Feedback Stabilisation.